Current Biology 24, 1126–1132, May 19, 2014 ©2014 Elsevier Ltd All rights reserved http://dx.doi.org/10.1016/j.cub.2014.03.050

Report

Contact Angle at the Leading Edge Controls Cell Protrusion Rate

Chiara Gabella,[1,*] Elena Bertseva,[1,2] Céline Bottier,[1] Niccolò Piacentini,[1] Alicia Bornert,[1] Sylvia Jeney,[2] László Forró,[2] Ivo F. Sbalzarini,[3] Jean-Jacques Meister,[1] and Alexander B. Verkhovsky[1]

[1]Laboratory of Cell Biophysics, Ecole Polytechnique Fédérale de Lausanne, 1015 Lausanne, Switzerland

[2]Laboratory of Physics of Complex Matter, Ecole Polytechnique Fédérale de Lausanne, 1015 Lausanne, Switzerland

[3]MOSAIC Group, Max Planck Institute of Molecular Cell Biology and Genetics, 01307 Dresden, Germany

Summary

Plasma membrane tension and the pressure generated by actin polymerization are two antagonistic forces believed to define the protrusion rate at the leading edge of migrating cells [1–5]. Quantitatively, resistance to actin protrusion is a product of membrane tension and mean local curvature (Laplace's law); thus, it depends on the local geometry of the membrane interface. However, the role of the geometry of the leading edge in protrusion control has not been yet investigated. Here, we manipulate both the cell shape and substrate topography in the model system of persistently migrating fish epidermal keratocytes. We find that the protrusion rate does not correlate with membrane tension, but, instead, strongly correlates with cell roundness, and that the leading edge of the cell exhibits pinning on substrate ridges—a phenomenon characteristic of spreading of liquid drops. These results indicate that the leading edge could be considered a triple interface between the substrate, membrane, and extracellular medium and that the contact angle between the membrane and the substrate determines the load on actin polymerization and, therefore, the protrusion rate. Our findings thus illuminate a novel relationship between the 3D shape of the cell and its dynamics, which may have implications for cell migration in 3D environments.

Results and Discussion

To investigate the relationship between membrane tension, actin-driven protrusion, and the 3D shape of the cell, we utilize the model system of fish epithelial keratocytes, which are characterized by a remarkably stable shape and constant high protrusion rate [6].

Membrane Tension and Cell Velocity

We measured membrane tension by using an optical trap [3, 7, 8] to pull tethers (actin-free membrane tubes; Figure S1 available online) from the membrane at the leading edge of migrating cells (Figures 1A and 1B and Movie S1). Tether forces varied among cells with a symmetrical single-maximum distribution peaking at approximately 40 pN (Figure 1C). In a few cases, when tethers were pulled from the back of the same cell, similar forces were observed, except for blebbistatin treated cells, in which forces at the front were reproducibly higher (Figure S2G). Consistent with this result, a recent theoretical study [9] predicted a difference in tension between front and back, which was expected to be more pronounced in the cells with smaller adhesions, as blebbistatin-treated cells.

A recent study reported that membrane tension in keratocytes is largely determined by cytoskeletal forces [10], but the cytoskeletal dynamics may be, in turn, affected by membrane tension. We tested how membrane resistance affects protrusion rate. Membrane tension is believed to counteract protrusion. Previous studies implicated membrane tension in control of cell spreading [3, 4, 11], in limiting the lateral extension of the cell [5], in confining protrusion to a single leading edge [1, 2], and in crushing the actin network during retraction at the cell rear [12]. However, membrane tension correlates positively with protrusion rate in *C. elegans* sperm [13], cells that migrate using the assembly of the major sperm protein instead of actin.

To modulate membrane tension and protrusion rate in migrating keratocytes, we used osmotic treatments and the inhibition of myosin-dependent contractility. Hypotonic conditions were expected to cause cell swelling and increase membrane tension, thus decreasing protrusion velocity, whereas hypertonic treatments were expected to have the opposite effect. Inhibition of myosin II with blebbistatin was shown to reduce cell velocity [14], and it was anticipated to increase tension through compromising retraction at the rear and stretching of the cell [5, 10, 15]. We observed that these treatments significantly affected cell velocity (Figures 2A and 2B and Movie S2); however, contrary to expectations, hypotonic treatment increased velocity, whereas hypertonic treatment decreased it. Consistent with previous reports [5, 14, 15], blebbistatin treatment reduced cell velocity. Interestingly, hypotonic treatment of blebbistatin-treated cells rescued cell velocity to the level of control cells (Movie S3). Surprisingly, despite marked changes in cell velocity, mean tether forces were not significantly affected by the above treatments (Figures 2C and S2), and no correlation was found between individual cell velocities and tether forces (Figure 2D). These results indicate that membrane tension by itself was not a factor mediating cell velocity changes.

Cell Shape and Velocity

According to Laplace's law, the difference of pressure across the membrane is a product of membrane tension and surface curvature. Thus, mechanical resistance to actin protrusion would depend not only on membrane tension, but also on the shape of the membrane interface, and changing this shape may modify the balance even in the absence of changes in tension. Therefore, we examined whether the shape of the cell was affected by the treatments. Measurement of vertical cell profiles with the fluorescence displacement method [16] indeed revealed significant shape change. Hypotonic treatment caused persistent swelling of both the lamellipodium and cell body in the vertical dimension (Figures 3A and 3F). Upon swelling, keratocytes with rough lamellipodia outlines frequently became more regular and coherent [5], but otherwise the change of shape happened without significant

*Correspondence: chiara.gabella@epfl.ch

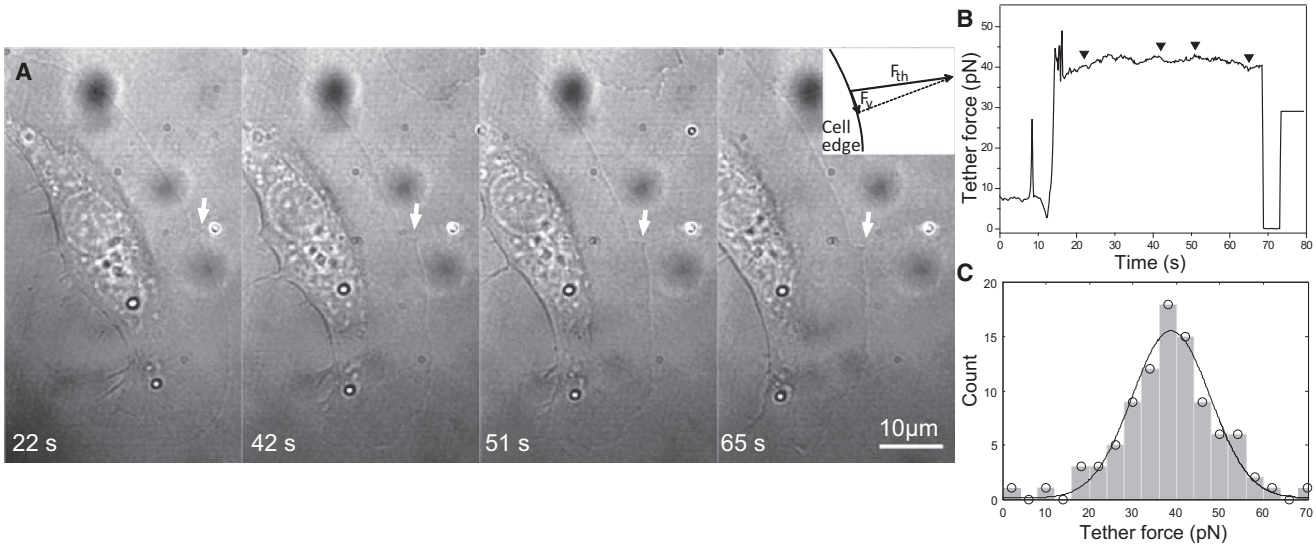

Figure 1. Measurement of Membrane Tension with a Tether Pulling Assay

(A) Time sequence of tether formation during pulling of a 1 μm diameter bead; white arrows indicate the attachment point of the tether to the cell front. The inset illustrates that the force component parallel to the cell edge (F_y) is small compared to the measured longitudinal tether force (F_{th}). Note that as the tether is pulled, its base travels along the perimeter of the cell, forming a characteristic step at the edge.

(B) Tether force as a function of time during pulling. Force remains constant during tether elongation. Arrowheads indicate the time points shown as snapshots in (A).

(C) Histogram of the measured tether forces in a population of keratocytes. Forces show a normal distribution.

See also Figure S1 and Movie S1.

rearrangement of the actin filament network, actin flow pattern, adhesion, or traction force distribution (Figures 3B–3E). Low retrograde flow velocity (Figure 3C) and the band of close substrate contact at the front (Figure 3D) suggested that the tip of the lamellipodial actin network maintained strong adhesion to the substrate. To quantitatively characterize shape change, we used a nondimensional parameter that we termed "roundness index." It was defined as the ratio of the projection area of a sphere of the same volume as the cell to the projection area of the cell. This parameter describes how similar the cell is to a sphere in the vertical dimension, but is not sensitive to changes of the cell aspect ratio in the substrate plane as long as the volume and the projection area remain the same. As expected, we observed a

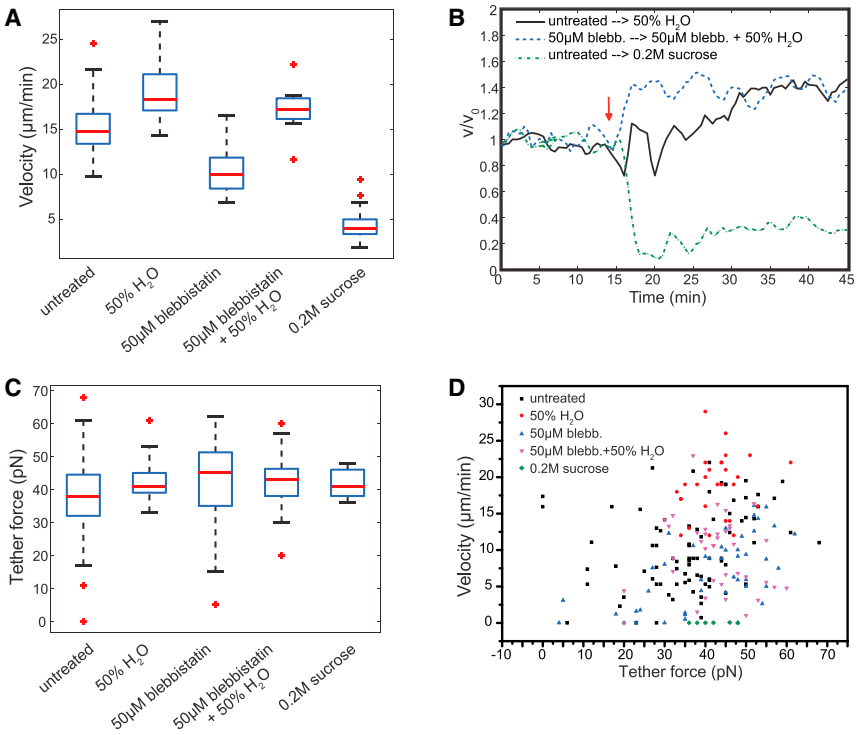

Figure 2. Protrusion Velocity and Tether Force for Cells under Various Treatments

(A and C) Boxplots of protrusion velocity (A) and tether force (C). For each box, the central red line is the median, the edges of the box are the 25th and 75th percentiles, the whiskers (black dashed lines) extend to the most extreme data points not considered outliers, and outliers are plotted individually (red crosses).

(B) Evolution of the protrusion velocity in individual cells over time during solution changes as indicated on the graph. Protrusion velocity (v) of each cell is normalized by the velocity of the same cell before the change of solution (v_0). The red arrow indicates the moment of change. Cells responded to osmotic treatments by a rapid and persistent change of velocity, suggesting that the effects were associated with the osmotic shock itself, rather than with subsequent adaptation to it.

(D) Scatter plot of velocity versus tether force for individual cells shows no evident correlation.

See also Figure S2 and Movies S2 and S3.

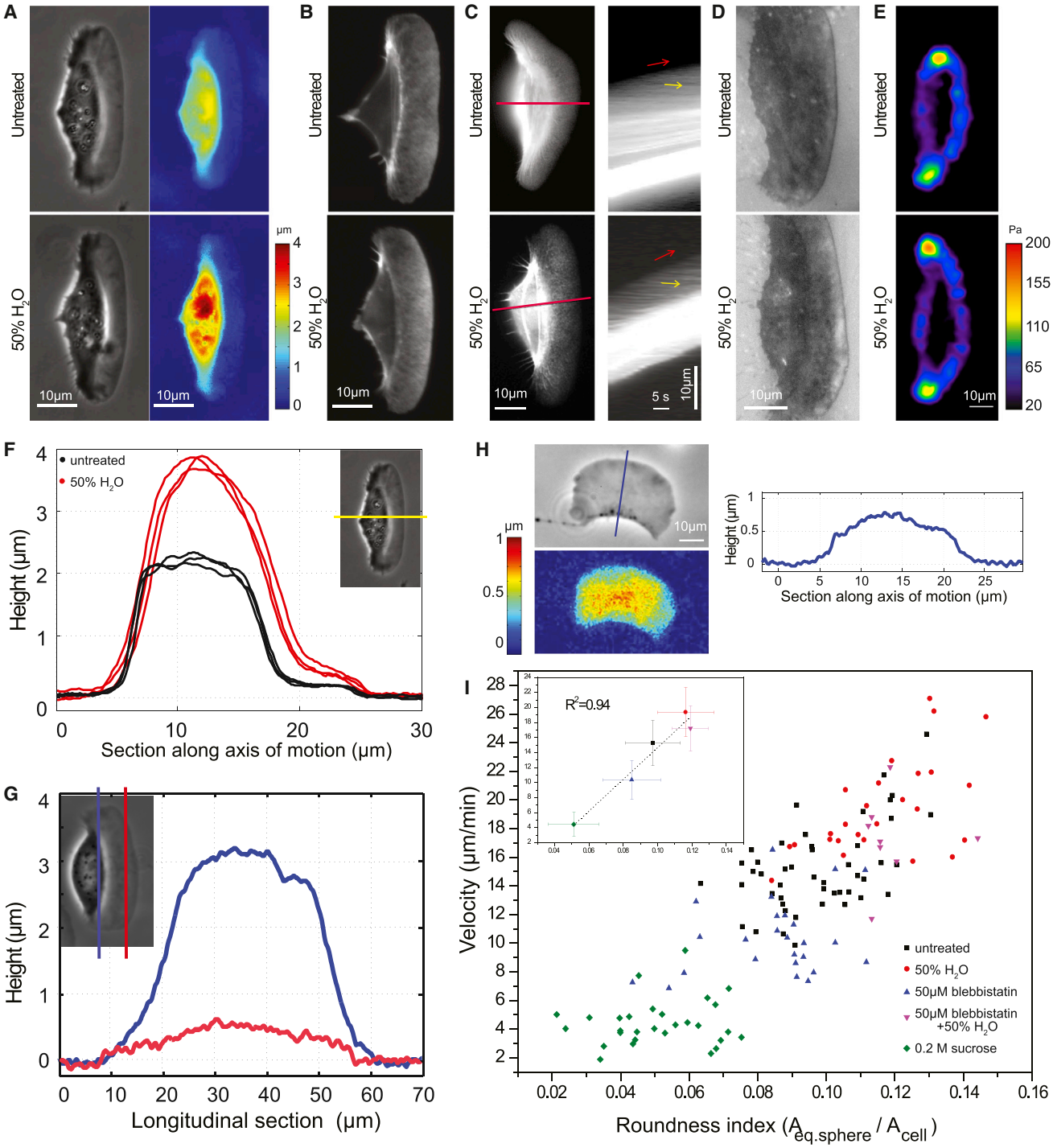

Figure 3. Cell Morphology and Dynamics under Various Treatments

(A–E) cells in isotonic (top) and hypotonic (bottom) solution.

(A) Phase-contrast (left) and fluorescence-displacement (right) images of the same cell before (top) and 10 min after (bottom) hypo-osmotic shock. The color scale indicates the height of the cell.

(B) Fluorescence images of cells stained for F-actin with rhodamine phalloidin.

(C) Fluorescence speckle microscopy of actin network flow in keratocytes injected with rhodamin-phalloidin. On the right are kymographs of the image sequences of the cells shown on the left; red lines in cell images indicate the positions where kymographs were taken. Forward movement of the cell edge is indicated in kymographs with red arrows, and actin retrograde flow is indicated with yellow arrows.

(D) Interference reflection microscopy (IRM) of the cells showing adhesion patterns. Dark bands at the leading edge indicate a close contact of the lamellipodia with the substrate.

(E) Traction force microscopy images showing substrate stress distribution for the same cell before (top) and after (bottom) a hypo-osmotic shock.

(F) Height profiles of the same cell as presented in (A) in isotonic medium (black lines) and 12 min after transition to a hypotonic solution (red lines). Profiles are taken along the axis of motion. The section is displayed as a yellow line in the inset, and the time interval between profiles in each condition is 30 s.

(legend continued on next page)

significant change of roundness due to treatments: hypotonically swollen cells were the roundest and hypertonically shrunken cells were the flattest, whereas control and blebbistatin-treated cells occupied intermediate positions, with blebbistatin-treated cells being slightly flatter than the control (Figure 3I, inset). Thus, the cells responded to the change of tonicity and to the inhibition of contractility with the change of shape rather than of membrane tension. Approximating the cell shape by a spherical segment, we estimated overall cell curvature and the pressure difference across the membrane corresponding to this curvature (see the Supplemental Experimental Procedures). The pressure difference was in the order of a few newtons per square meter, which is very small compared to the initial difference in osmotic pressure between the cell and the hypotonic or hypertonic external media. Thus, the cell accommodates most of the osmotic pressure difference by changing its volume, and the small residual hydrostatic pressure is carried by the membrane through a change in curvature, but without any significant change in tension [17]. Similarly, blebbistatin treatment may decrease intracellular pressure by blocking contractility [18], and this change of pressure is accommodated largely by flattening of the membrane, rather than by tension changes.

Cell roundness as defined above exhibited strong positive correlation with the cell velocity (Figure 3I). A similar correlation was observed with the cell volume (Figure S3A), which was itself correlated with the cell roundness. Other parameters describing cell shape, such as projection area or aspect ratio [5], did not display such a correlation (Figures S3B and S3C).

Contact Angle and Cell Velocity

We considered and discounted possible causes of protrusion-roundness correlation related to adhesion, changing of actin monomer pool, or cytoplasm viscosity (see the Supplemental Discussion). On the other hand, cell rounding can influence protrusion by changing the shape of the membrane interface at the leading edge and thus modifying the force load on actin assembly. To account for the role of membrane shape in the force balance, we consider a simplified model inspired by the Young-Laplace description of wetting phenomena (Figure 4A). We assume that actin assembly exerts pressure against a narrow band of the membrane along the cell front edge. We consider this band to be infinitely thin, and consequently we express actin assembly force as tension, i.e., force per unit length of the edge. Then, leading edge can be described as a triple interface line to which actin tension, γ_{actin}, and the tensions originating from three interfaces (apical membrane with the medium, γ; ventral membrane with the substrate, $\gamma_{c/s}$; and substrate with the medium, $\gamma_{m/s}$) are applied. γ_{actin} and the interfacial tensions, $\gamma_{c/s}$ and $\gamma_{m/s}$, are oriented along the substrate surface, while γ (i.e., membrane tension) is directed according to the contact angle formed by the membrane with the substrate. This overall geometry is consistent with IRM images showing no significant gap between the membrane and the substrate at the leading edge (Figure 4B; also see the Supplemental Experimental Procedures for the definition of the effective contact angle). The effective contact angle ϑ at the triple interface should satisfy a force balance between interfacial tensions and actin assembly tension:

$$\gamma_{actin} = \gamma \cos \vartheta + \left(\gamma_{c/s} - \gamma_{m/s}\right).$$

In our experiments, substrate properties were not modified; therefore, the interfacial tensions, $\gamma_{c/s}$ and $\gamma_{m/s}$, most likely remained constant, and membrane tension, γ, was found not to change significantly upon treatments. Changing the contact angle would mean changing the projection of the membrane tension onto the substrate plane, effectively changing the load against which actin polymerizes. Increasing the contact angle would decrease the load and therefore accelerate actin assembly and protrusion, whereas decreasing the angle would increase the load and slow down protrusion. Actin assembly may then tune itself to a contact angle, allowing force balance to be achieved over a range of contact angles, with different angles corresponding to different protrusion rates. Consistent with this mechanism, our observations indicate that tuning of the protrusion velocity occurs locally at the leading edge without changes in the overall actin dynamics, adhesion distribution, or traction force pattern (Figures 3B–3E). Effects at the triple interface generate traction forces during liposome spreading [19], but in keratocytes these forces are mostly due to actomyosin contractility [15].

Assuming that the apical membrane is not strongly attached to the cytoskeleton, the contact angle could be defined by the global curvature of the membrane which, in turn, is due to the balance between membrane tension and the pressure difference between cytoplasm and extracellular medium. This assumption is motivated by the finding that the tether base moved freely along the cell edge (Figure 1A and Movie S1), indicating little or no interaction of the membrane with the cytoskeleton [17], and by the observation of a convex-up shape of the vertical profile of the lamellipodium (see Figures 3F and S3D). Note that this shape was not due to the presence of the cell body, as lamellar fragments of keratocytes exhibited similar convex profile (Figure 3H). In the case of fragments, however, the profile was symmetrical, without the large bulge at the back due to the nucleus and the organelles contained in the cell body. When the cytoplasm is pressurized by hypotonic treatment or myosin-dependent contraction, the hydrostatic pressure difference across the membrane rounds up the apical cell surface, increasing the contact angle at the leading edge and effectively removing part of the actin assembly load. It could be speculated that if the cell is inflated to such an extent that actin assembly becomes completely unloaded, protrusion could switch to an actin-independent, blebbing regime [20], which we occasionally observed in hypotonically treated cells (Movie S5).

Contact angle may not only change due to a change in membrane curvature, but also to a change of the substrate topography. In wetting phenomena, this effect produces a characteristic behavior known as pinning of the droplet interface on substrate ridges [21]. Pinning happens because over a range of contact angles, unbalanced forces drive the interface back to the surface ridges. We fabricated a substrate

(G) Cell height longitudinal profiles taken along the lines shown in the inset.
(H) Phase-contrast (top) and fluorescence-displacement (bottom) images of a cytoplasmic fragment of keratocyte. The color scale indicates the height of the fragment. On the right is a height profile of the fragment taken along the blue line in the phase-contrast image.
(I) A plot of protrusion velocity versus cell roundness index for different treatments shows a positive linear correlation. The inset shows averaged values for each treatment. Data represent the mean ± SD, and the correlation coefficient is indicated in the graph.
See also Figure S3.

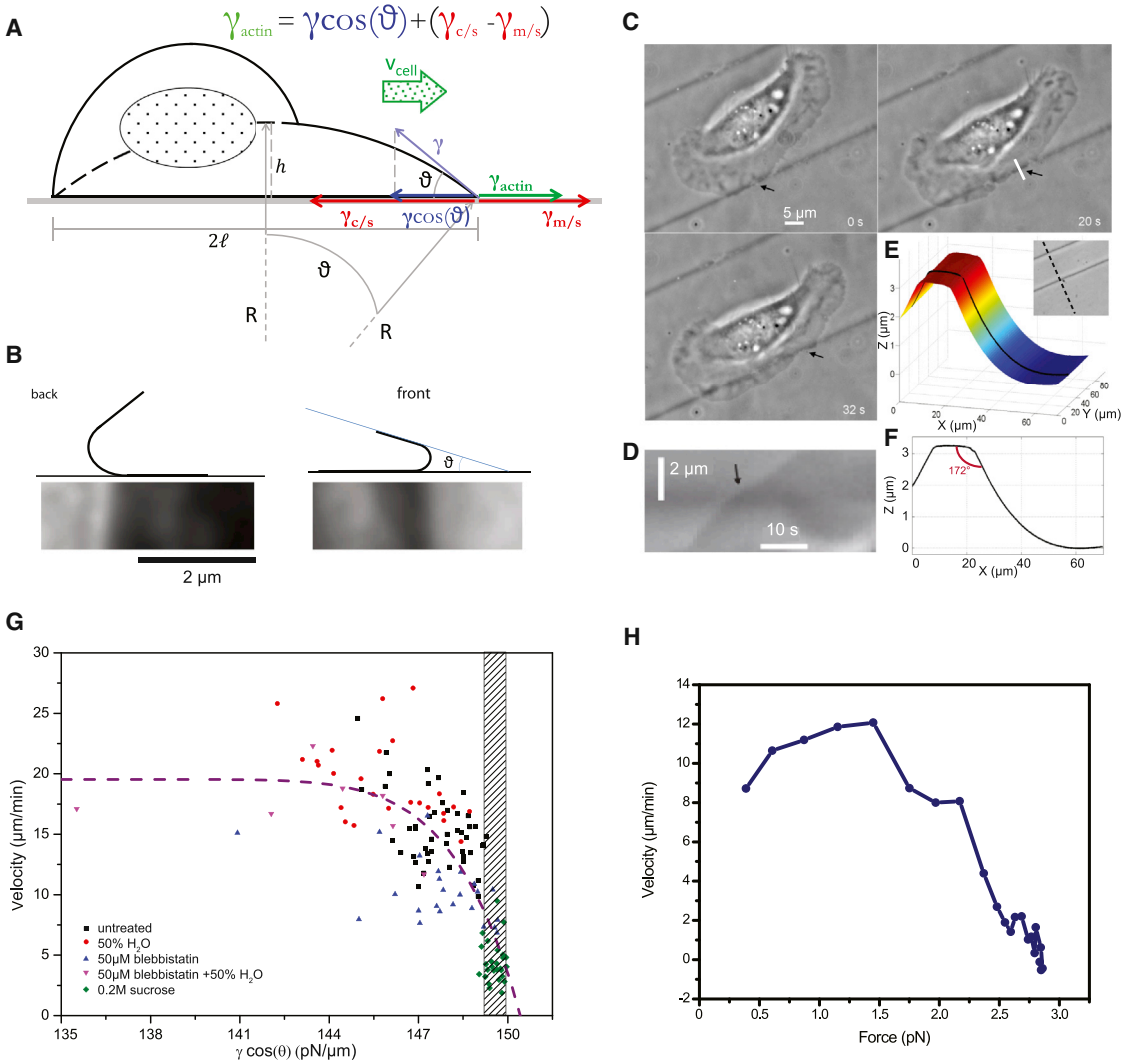

Figure 4. Contact Angle and Force-Velocity Relationship for Leading Edge Protrusion

(A) Diagram of the force balance for the triple interface at the leading edge showing the contributing forces and dimensions used for determining membrane curvature and contact angle (see the main text). Lamellipodium height is exaggerated for clarity. The thick green arrow indicates the direction of cell motion. At the top, the equation of the force balance is shown.

(B) Diagrams illustrating the definition of effective contact angle aligned with the IRM images of the leading and trailing cell edges shown at comparable magnifications. At the leading edge, the microscopic membrane curvature radius is small so that no gap is detected by IRM between the ventral membrane and the substrate; in contrast, at the rear edge, the gap is apparent as a light fringe in the image.

(C) Image sequence of a keratocyte moving on a substrate with ridges. Black arrows show pinning of parts of the leading edge at the ridge.

(D) Kymograph generated from the solid white line of the top-right panel of (C) displaying slowing of the cell edge at the ridge (black arrow).

(E) Tridimensional view of the substrate ridge generated by atomic force microscopy imaging. The inset shows a phase-contrast image of the substrate; the black dashed line corresponds to the black line on the 3D rendering.

(F) Vertical profile of the substrate along the black line in (E). Ridge angle is indicated.

(G) Plot of protrusion velocity versus membrane load estimated from the contact angle at the leading edge for cells under different conditions. The dark band represents the interval of load values estimated for the lateral extremities of the cells, where protrusion stalls. For help visualizing the trend, data are fitted (dashed line) according to [5], in the form of $v = v_0(1 - ((\gamma \cos\theta - 90)/F_s)^w)$, with $w = 7.10$, $F_s = 10.28$ pN/μm, and $v_0 = 19.54$ μm/min.

(H) Experimental force-velocity relationship for the leading edge obtained with a trapped bead of 0.8 μm diameter positioned in the way of a moving keratocyte so that advancing cell edge pushed the bead from the center of the trap.

See also Movies S4 and S5.

with very blunt and soft ridges (Figures 4E and 4F and the Supplemental Experimental Procedures) and observed that when the leading edge reached the ridges, protrusion stopped momentarily, resulting in a segment of the leading edge "pinned" to the ridge (Figures 4C and 4D). This predicted pinning behavior validates the idea that the leading edge behaves as a triple interface and also suggests a general mechanism for how protrusion could be modulated by substrate topography.

Cell velocities for various treatments were plotted versus loads based on the contact angles (Figure 4G) estimated by measurement of cell height and horizontal length in the direction of motion (see the Supplemental Experimental Procedures). Obtained relationship exhibits a concave-down shape

typical of force-velocity curves for actin protrusion at the leading edge [22, 23]. Maximal membrane load would occur at zero contact angle and is estimated at approximately 150 pN/μm (see the Supplemental Experimental Procedures) or in the order of 1 pN per filament assuming filament density in the order of 100 per micrometer [24, 25]. Part of the membrane load may be balanced by interfacial tensions at the substrate. To estimate this part, we eliminated cytoskeletal forces by treating the cells with blebbistatin and cytochalasin D. As expected, these cells did not move. They exhibited contact angles similar to those of control cells, but significantly lower membrane tension of 35 pN/μm (tether force ≈20 pN; Figure S2F). This tension should be balanced by the sum of membrane-substrate and substrate-medium tensions (effectively, adhesion). Combined blebbistatin and cytochalasin treatment most likely greatly reduced adhesion [26]; consequently, the contribution of interfacial forces in untreated cells is expected to be more significant.

Irrespective of the absolute value of the total load, Figure 4G suggests that a sharp change in protrusion velocity results from changing the load by just a few piconewtons per micrometer, a trend previously observed experimentally and predicted theoretically [22, 23, 27–30]. We confirmed this feature by directly measuring the force-velocity relationship by applying the load with optical trap (Figure 4H, Movie S4, and the Supplemental Experimental Procedures). The resulting range of load was similar to the one estimated from the contact angle (Figure 4G).

To test whether this apparent sensitivity of protrusion velocity to the load through the contact angle may be responsible for local velocity variations, we estimated the contact angles and corresponding loads at the lateral extremities of the cell approximating the apical cell surface with an ellipsoidal cap (where surface curvature and contact angles are smaller in the direction of the long axis than along the short axis; see the Experimental Procedures). Interestingly, the estimated contact angles at the lateral extremities of the cell corresponded to actin assembly loads similar to the front loads of hypertonically treated cells, i.e., they were found in the region of the force-velocity curve where the velocity dropped sharply (darkened interval in Figure 4G). This is consistent with the arrest of protrusion at the lateral sides of the cell [5, 31, 32]. Thus, decreasing contact angle by flattening the apical membrane could be a mechanism contributing to local protrusion regulation. In contrast to protrusion control based on a change in membrane tension [1–3], which is likely to affect the entire cell, regulation through contact angle depends on local cell geometry.

Our study underscores the fundamental importance of membrane configuration and contact angle for cellular force balance and edge dynamics. Complementing previous studies on the role of membrane tension in protrusion control [1–5, 11–13], here we suggest that membrane configuration could locally control actin protrusion even if membrane tension is constant and uniform around the cell. For nonliving matter, contact angle has long proven an important physical concept, explaining various phenomena at liquid-solid interfaces, including, interestingly, motion driven by contact angle anisotropy, as observed in autophobic droplet spreading [33] and durotaxis [34], where the droplets even assume shapes reminiscent of migrating cells. We extend the contact angle concept to the migration of living cells by taking into account active cytoskeletal forces present at the cell edge. Our study provides a novel framework for understanding the relationship between global cell shape and local dynamics, the balance between lamellipodia protrusion and blebbing, and the modulation of cell shape and motion by substrate topology. To isolate the effects of the contact angle, we have focused on cell and substrate geometry, intentionally neglecting other important parameters, such as adhesive properties and contractile forces at the edge. Future studies may relate contact angle, protrusive forces at the front, contractile forces at the back, adhesive properties, membrane tension, pressure, and global cell shape in a single physical model.

Experimental Procedures

Fish epidermal keratocytes were cultured and imaged as previously described [14, 16, 25]. Details of the optical trap assays, microfabrication, atomic force microscopy, traction force microscopy, and cell shape analysis are provided in the Supplemental Experimental Procedures. Experiments with fish keratocytes were approved by the Cantonal Veterinary Office (authorization number 2505.0) in agreement with the law on animal protection in Switzerland.

Supplemental Information

Supplemental Information includes Supplemental Discussion, three figures, Supplemental Experimental Procedures, and five movies and can be found with this article online at http://dx.doi.org/10.1016/j.cub.2014.03.050.

Acknowledgments

We thank B. Vianay, M. Ambühl, F. Raynaud, and C. Labouesse (LCB, EPFL) for stimulating discussions and J. Smith-Clerc (LCB, EPFL) for technical help. This work was supported by Swiss National Science Foundation grant 31003A-135661 to A.B.V. C.G. was funded by an iPhD fellowship from the Swiss SystemsX.ch initiative to A.B.V. and I.F.S.

Received: August 13, 2013
Revised: February 4, 2014
Accepted: March 18, 2014
Published: May 1, 2014

References

1. Houk, A.R., Jilkine, A., Mejean, C.O., Boltyanskiy, R., Dufresne, E.R., Angenent, S.B., Altschuler, S.J., Wu, L.F., and Weiner, O.D. (2012). Membrane tension maintains cell polarity by confining signals to the leading edge during neutrophil migration. Cell *148*, 175–188.
2. Mogilner, A., and Zhu, J. (2012). Cell polarity: tension quenches the rear. Curr. Biol. *22*, R48–R51.
3. Raucher, D., and Sheetz, M.P. (2000). Cell spreading and lamellipodial extension rate is regulated by membrane tension. J. Cell Biol. *148*, 127–136.
4. Gauthier, N.C., Fardin, M.A., Roca-Cusachs, P., and Sheetz, M.P. (2011). Temporary increase in plasma membrane tension coordinates the activation of exocytosis and contraction during cell spreading. Proc. Natl. Acad. Sci. USA *108*, 14467–14472.
5. Keren, K., Pincus, Z., Allen, G.M., Barnhart, E.L., Marriott, G., Mogilner, A., and Theriot, J.A. (2008). Mechanism of shape determination in motile cells. Nature *453*, 475–480.
6. Mogilner, A., and Keren, K. (2009). The shape of motile cells. Curr. Biol. *19*, R762–R771.
7. Dai, J., and Sheetz, M.P. (1995). Mechanical properties of neuronal growth cone membranes studied by tether formation with laser optical tweezers. Biophys. J. *68*, 988–996.
8. Raucher, D. (2008). Chapter 17: application of laser tweezers to studies of membrane-cytoskeleton adhesion. Methods Cell Biol. *89*, 451–466.
9. Schweitzer, Y., Lieber, A.D., Keren, K., and Kozlov, M.M. (2014). Theoretical analysis of membrane tension in moving cells. Biophys. J. *106*, 84–92.
10. Lieber, A.D., Yehudai-Resheff, S., Barnhart, E.L., Theriot, J.A., and Keren, K. (2013). Membrane tension in rapidly moving cells is determined by cytoskeletal forces. Curr. Biol. *23*, 1409–1417.

11. Masters, T.A., Pontes, B., Viasnoff, V., Li, Y., and Gauthier, N.C. (2013). Plasma membrane tension orchestrates membrane trafficking, cytoskeletal remodeling, and biochemical signaling during phagocytosis. Proc. Natl. Acad. Sci. USA *110*, 11875–11880.
12. Ofer, N., Mogilner, A., and Keren, K. (2011). Actin disassembly clock determines shape and speed of lamellipodial fragments. Proc. Natl. Acad. Sci. USA *108*, 20394–20399.
13. Batchelder, E.L., Hollopeter, G., Campillo, C., Mezanges, X., Jorgensen, E.M., Nassoy, P., Sens, P., and Plastino, J. (2011). Membrane tension regulates motility by controlling lamellipodium organization. Proc. Natl. Acad. Sci. USA *108*, 11429–11434.
14. Schaub, S., Bohnet, S., Laurent, V.M., Meister, J.J., and Verkhovsky, A.B. (2007). Comparative maps of motion and assembly of filamentous actin and myosin II in migrating cells. Mol. Biol. Cell *18*, 3723–3732.
15. Fournier, M.F., Sauser, R., Ambrosi, D., Meister, J.J., and Verkhovsky, A.B. (2010). Force transmission in migrating cells. J. Cell Biol. *188*, 287–297.
16. Bottier, C., Gabella, C., Vianay, B., Buscemi, L., Sbalzarini, I.F., Meister, J.J., and Verkhovsky, A.B. (2011). Dynamic measurement of the height and volume of migrating cells by a novel fluorescence microscopy technique. Lab Chip *11*, 3855–3863.
17. Pietuch, A., Brückner, B.R., and Janshoff, A. (2013). Membrane tension homeostasis of epithelial cells through surface area regulation in response to osmotic stress. Biochim. Biophys. Acta *1833*, 712–722.
18. Stewart, M.P., Helenius, J., Toyoda, Y., Ramanathan, S.P., Muller, D.J., and Hyman, A.A. (2011). Hydrostatic pressure and the actomyosin cortex drive mitotic cell rounding. Nature *469*, 226–230.
19. Murrell, M.P., Voituriez, R., Joanny, J.-F., Nassoy, P., Sykes, C., and Gardel, M.L. (2014). Liposome adhesion generates traction stress. Nat. Phys. *10*, 163–169.
20. Charras, G., and Paluch, E. (2008). Blebs lead the way: how to migrate without lamellipodia. Nat. Rev. Mol. Cell Biol. *9*, 730–736.
21. Kalinin, Y.V., Berejnov, V., and Thorne, R.E. (2009). Contact line pinning by microfabricated patterns: effects of microscale topography. Langmuir *25*, 5391–5397.
22. Heinemann, F., Doschke, H., and Radmacher, M. (2011). Keratocyte lamellipodial protrusion is characterized by a concave force-velocity relation. Biophys. J. *100*, 1420–1427.
23. Prass, M., Jacobson, K., Mogilner, A., and Radmacher, M. (2006). Direct measurement of the lamellipodial protrusive force in a migrating cell. J. Cell Biol. *174*, 767–772.
24. Abraham, V.C., Krishnamurthi, V., Taylor, D.L., and Lanni, F. (1999). The actin-based nanomachine at the leading edge of migrating cells. Biophys. J. *77*, 1721–1732.
25. Schaub, S., Meister, J.J., and Verkhovsky, A.B. (2007). Analysis of actin filament network organization in lamellipodia by comparing experimental and simulated images. J. Cell Sci. *120*, 1491–1500.
26. Alexandrova, A.Y., Arnold, K., Schaub, S., Vasiliev, J.M., Meister, J.J., Bershadsky, A.D., and Verkhovsky, A.B. (2008). Comparative dynamics of retrograde actin flow and focal adhesions: formation of nascent adhesions triggers transition from fast to slow flow. PLoS ONE *3*, e3234.
27. Weichsel, J., and Schwarz, U.S. (2010). Two competing orientation patterns explain experimentally observed anomalies in growing actin networks. Proc. Natl. Acad. Sci. USA *107*, 6304–6309.
28. Shahapure, R., Difato, F., Laio, A., Bisson, G., Ercolini, E., Amin, L., Ferrari, E., and Torre, V. (2010). Force generation in lamellipodia is a probabilistic process with fast growth and retraction events. Biophys. J. *98*, 979–988.
29. Zimmermann, J., Brunner, C., Enculescu, M., Goegler, M., Ehrlicher, A., Käs, J., and Falcke, M. (2012). Actin filament elasticity and retrograde flow shape the force-velocity relation of motile cells. Biophys. J. *102*, 287–295.
30. Bohnet, S., Ananthakrishnan, R., Mogilner, A., Meister, J.J., and Verkhovsky, A.B. (2006). Weak force stalls protrusion at the leading edge of the lamellipodium. Biophys. J. *90*, 1810–1820.
31. Grimm, H.P., Verkhovsky, A.B., Mogilner, A., and Meister, J.J. (2003). Analysis of actin dynamics at the leading edge of crawling cells: implications for the shape of keratocyte lamellipodia. Eur. Biophys. J. *32*, 563–577.
32. Lee, J., Ishihara, A., Theriot, J.A., and Jacobson, K. (1993). Principles of locomotion for simple-shaped cells. Nature *362*, 167–171.
33. Hunter, J.K., Li, Z., and Zhao, H. (2002). Reactive Autophobic Spreading of Drops. J. Comput. Phys. *183*, 335–366.
34. Style, R.W., Che, Y., Park, S.J., Weon, B.M., Je, J.H., Hyland, C., German, G.K., Power, M.P., Wilen, L.A., Wettlaufer, J.S., and Dufresne, E.R. (2013). Patterning droplets with durotaxis. Proc. Natl. Acad. Sci. USA *110*, 12541–12544.